PHYSICAL REVIEW C **97**, 014303 (2018)

Cluster and toroidal aspects of isoscalar dipole excitations in ^{12}C

Yoshiko Kanada-En'yo,[*] Yuki Shikata, and Horiyuki Morita
Department of Physics, Kyoto University, Kyoto 606-8502, Japan

(Received 10 September 2017; published 5 January 2018)

We investigate cluster and toroidal aspects of isoscalar dipole excitations in ^{12}C based on the shifted basis antisymmetrized molecular dynamics combined with the generator coordinate method, which can describe 1p-1h excitations and 3α dynamics. In the $E = 10$-15 MeV region, we find two low-energy dipole modes separating from the giant dipole resonance. One is the developed 3α-cluster state and the other is the toroidal dipole mode. The cluster state is characterized by the high-amplitude cluster motion beyond the 1p-1h model space, whereas the toroidal dipole mode is predominantly described by 1p-1h excitations in the ground state. The low-energy dipole states are remarkably excited by the toroidal dipole operator, which can measure the nuclear vorticity. For compressive dipole transition strengths, a major part is distributed in the 30- to 50-MeV region for the giant dipole resonance, and 5% of the total energy-weighted sum exists in the $E < 20$ MeV region.

DOI: 10.1103/PhysRevC.97.014303

I. INTRODUCTION

In recent decades, research on isoscalar monopole (ISM) and isoscalar dipole (ISD) excitations has been proceeding remarkably through experiments with α inelastic scattering. Recently, particular attention has been paid to low-energy (LE) monopole and dipole strengths below the giant resonances. Since the ISM and ISD operators corresponding to compressive modes can directly excite intercluster motions, they are good probes for cluster states as discussed by Yamada *et al.* [1] and Chiba *et al.* [2]. Indeed, in nuclei such as ^{16}O and ^{24}Mg, the LE-ISM and -ISD strengths are described by cluster states, which appear separating from the collective modes of the giant resonances.

In the progress in physics of unstable nuclei, LE-ISD excitations have also been discussed in relation to isovector (IV) dipole excitations (see, e.g., reviews in Refs. [3–6] and references therein). Owing to experimental studies with hadronic probes, information on isospin characters of LE dipole (LED) excitations is becoming available for various nuclei. Isoscalar (IS) giant dipole resonances (GDRs), which correspond to the collective compressive dipole mode, have been observed for stable nuclei in the energy region higher than that of the IVGDRs for the proton-neutron opposite oscillation mode. Below the ISGDRs, significant LE-ISD strengths are known in stable nuclei [7–9]. For the ISD strengths of ^{16}O and ^{40}Ca, 4%–5% of the energy-weighted sum (EWS) rule has been observed in the $E \leqslant 10$ MeV region.

In order to understand the LED strengths, the toroidal dipole (TD) mode (also called the torus or vortical mode) has been proposed with hydrodynamical models [10,11]. The TD mode carries vorticity and its character is much different from that of the compressive dipole (CD) mode, which corresponds to the ordinary ISD mode contributing to the ISGDR. The energy of the TD mode is expected to be lower than the ISGDR energy because it conserves the nuclear density. Nowadays, microscopic calculations with the quasiparticle phonon model and random phase approximation have been obtained, and the toroidal natures of the LED excitations in various nuclei have been investigated [3,12–17].

For the ISD strengths of ^{12}C measured by α inelastic scattering, several percent of the EWS rule has been observed in the $E \leqslant 20$ MeV region below the ISGDR energy [18]. Among the LE-ISD strengths, there is a peak for the 1_1^- state at 10.8 MeV. In addition, another peak (or bump) structure around 15 MeV exists, indicating the possible existence of an LED mode other than the 1^- state (10.8 MeV). In theoretical studies of ^{12}C, a variety of 3α-cluster states have been suggested in excited states above the 3α threshold energy (7.16 MeV). Microscopic 3α-cluster models [19–22] describe a spatially developed 3α-cluster structure of the 1_1^- state. Even though cluster models are useful for 3α-cluster states of ^{12}C, the models *a priori* assume three α clusters, and therefore they are insufficient to study 1p-1h excitations and unable to describe giant resonances. In order to take into account coherent 1p-1h excitations for the giant resonances as well as the high-amplitude cluster modes, one of the authors, Y.K-E., has extended the antisymmetrized molecular dynamics (AMD) [23–26] and constructed a new method, the shifted basis AMD (sAMD) combined with the generator coordinate method (GCM) with respect to the intercluster motion, which we call the "sAMD + GCM" [27–29]. In the previous work [29], we applied the sAMD + GCM to calculate the ISM and ISD transition strengths of ^{12}C and obtained significant LE-ISD strengths in the $E = 10$-15 MeV region well separated from the high-energy strengths for the ISGDR.

Our aim in this paper is to clarify the natures of the LE-ISD excitations of ^{12}C, in particular, cluster and toroidal aspects, by reanalysis of the previous calculation. To probe the toroidal nature, we adopt the TD operator in addition to the CD operator for the ordinary ISD and show remarkable TD strengths for two

---

[*] yenyo@ruby.scphys.kyoto-u.ac.jp

2469-9985/2018/97(1)/014303(9)

LE-ISD modes: the 1^-_1 mode, with the developed 3α cluster structure; and the 1^-_2 mode, dominated by 1p-1h configurations with significant cluster-breaking. We also discuss the TD mode from a cluster picture and its connection with 1p-1h excitations in the shell-model limit.

The paper is organized as follows. The framework of the sAMD + GCM for ^{12}C is explained in Sec. II. Definitions of ISD operators are given in Sec. III. Section IV reports the calculated results and discusses the properties of the LED modes. The intrinsic structure of the TD mode and its shell-model limit are presented in Sec. VI. Finally, the paper concludes with a summary and outlook in Sec. VII.

II. sAMD + GCM

The sAMD + GCM has been applied to ISM, ISD, and $E1$ excitations of light nuclei such as ^{10}Be, ^{12}C, and ^{16}O [27–29]. A similar method has recently been applied to $E1$ and ISD excitations of ^{26}Ne by Kimura [30]. In the previous work, we applied the sAMD + GCM to ^{12}C by taking into account 3α-cluster configurations. For the detailed procedure of the sAMD + GCM calculation, the reader is referred to Ref. [29].

In the AMD method, a basis wave function is given by a Slater determinant,

$$\Phi_{\rm AMD}(\boldsymbol{Z}) = \frac{1}{\sqrt{A!}}\mathcal{A}\{\varphi_1,\varphi_2,\ldots,\varphi_A\}, \tag{1}$$

where $\mathcal{A}$ is the antisymmetrizer, and φ_i is the ith single-particle wave function written by a product of spatial, spin, and isospin wave functions,

$$\varphi_i = \phi_{\boldsymbol{X}_i}\chi_i\tau_i, \tag{2}$$

$$\phi_{\boldsymbol{X}_i}(\boldsymbol{r}_j) = \left(\frac{2\nu}{\pi}\right)^{3/4}\exp[-\nu(\boldsymbol{r}_j-\boldsymbol{X}_i)^2], \tag{3}$$

$$\chi_i = \left(\frac{1}{2}+\xi_i\right)\chi_\uparrow + \left(\frac{1}{2}-\xi_i\right)\chi_\downarrow, \tag{4}$$

where $\phi_{\boldsymbol{X}_i}$ and χ_i are the spatial and spin functions, respectively, and τ_i is the isospin function fixed to be a proton or neutron. The width parameter $\nu = 0.19\ \mathrm{fm}^{-2}$ is used to minimize the ground-state energy of ^{12}C. The AMD wave function is specified by a set of variational parameters, $\boldsymbol{Z} \equiv \{\boldsymbol{X}_1,\ldots,\boldsymbol{X}_A,\xi_1,\ldots,\xi_A\}$, which indicate Gaussian centroids and spin orientations of all single-particle wave functions.

In order to obtain the ground-state wave function, the variation is done after angular-momentum and parity projections (VAP) for the 0^+-projected AMD wave function as

$$\frac{\delta}{\delta \boldsymbol{X}_i}\frac{\langle\Phi|H|\Phi\rangle}{\langle\Phi|\Phi\rangle} = 0, \tag{5}$$

$$\frac{\delta}{\delta \xi_i}\frac{\langle\Phi|H|\Phi\rangle}{\langle\Phi|\Phi\rangle} = 0, \tag{6}$$

$$\Phi = P^{J\pi}_{MK}\Phi_{\rm AMD}(\boldsymbol{Z}), \tag{7}$$

where $P^{J\pi}_{MK}$ is the product of the angular-momentum and parity-projection operators, $P^J_{MK}P^\pi$. We denote the optimized parameter set $\boldsymbol{Z}$ for the ground state $\boldsymbol{Z}^0_{\rm VAP} = \{\boldsymbol{X}^0_1,\ldots,\boldsymbol{X}^0_A,\xi_1,\ldots,\xi^0_A\}$.

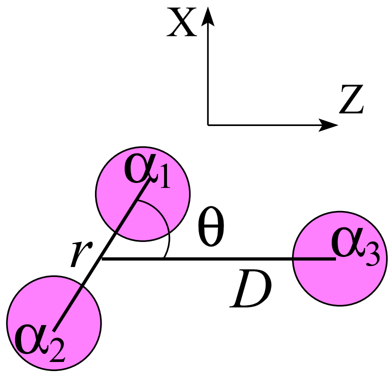

FIG. 1. Schematic of 3α configurations in the GCM for ^{12}C.

To take into account 1p-1h excitations on top of the obtained ground state, we consider small variations of single-particle wave functions of $\Phi_{\rm AMD}(\boldsymbol{Z}^0_{\rm VAP})$ by shifting the Gaussian centroid of the ith single-particle wave function, $\boldsymbol{X}^0_i \to \boldsymbol{X}^0_i + \epsilon\boldsymbol{e}_\sigma$, where ϵ is a small enough constant and $\boldsymbol{e}_\sigma$ ($\sigma = 1,\ldots,8$) are unit vectors for eight directions explained in Ref. [29]. As for the intrinsic spin of the shifted single-particle wave function, the spin nonflip and flip states are adopted. Consequently, totally $16A = 192$ wave functions of the spin nonflip and flip shifted AMD wave functions are superposed. We call this method the shifted basis AMD.

In addition to 1p-1h excitations expressed by the sAMD, we combine the GCM with the sAMD in order to take into account high-amplitude dynamics of three α clusters by superposing various 3α configurations written by the Brink-Bloch cluster-model wave functions [31]. Practically, a 3α-cluster configuration can be expressed with the AMD wave function by setting the parameters at $\boldsymbol{X}_i = \boldsymbol{S}_k$ for four nucleons ($p\uparrow$, $p\downarrow$, $n\uparrow$, and $n\downarrow$) in the kthα cluster (α_k). $\boldsymbol{S}_k$ indicates the α_k-cluster position and is given as

$$\boldsymbol{S}_1 = -\frac{1}{3}\boldsymbol{D} + \frac{\boldsymbol{r}}{2}, \tag{8}$$

$$\boldsymbol{S}_2 = -\frac{1}{3}\boldsymbol{D} - \frac{\boldsymbol{r}}{2}, \tag{9}$$

$$\boldsymbol{S}_3 = \frac{2}{3}\boldsymbol{D}. \tag{10}$$

Here the α_1-α_2 and α_3-$\alpha_1\alpha_2$ relative vectors, $\boldsymbol{r}$ and $\boldsymbol{D}$, are chosen to be $\boldsymbol{r} = (r\cos\theta, r\sin\theta, 0)$ and $\boldsymbol{D} = (0,0,D)$, respectively. θ is the angle between two vectors as shown in the schematic in Fig. 1. We use $r = \{0.8, 1.8, \ldots, 4.8\ \mathrm{fm}\}$, $D = \{1, 2, \ldots, 7\ \mathrm{fm}\}$, and $\theta = (\pi/8)i$ ($i = 0,\ldots,4$). Finally, in the sAMD + GCM, we superpose all the basis wave functions of the sAMD and 3α wave functions in addition to the original VAP wave function $[\Phi_{\rm AMD}(\boldsymbol{Z}^0_{\rm VAP})]$ as done in the previous work [29]. The final wave functions $\Psi(J^\pi_k)$ for the 0^+_k and 1^-_k states are expressed by superposition of the J^π-projected wave functions with coefficients determined by diagonalizing the norm and Hamiltonian matrices.

In the sAMD + GCM method, the ground state is obtained by the VAP, and therefore, it already contains the ground-state correlation beyond the mean-field approximation. In the sAMD, 1p-1h excitations in the ground state are taken into account by the linear combination of shifted Gaussian wave packets, and high-amplitude cluster motion is treated by superposition of 3α-cluster wave functions in the GCM. In the present method, the center-of-mass motion is exactly removed.

III. ISD OPERATORS AND TRANSITION STRENGTHS

In order to probe the vorticity of the nuclear current, two kinds of operators have been used. One is the "toroidal mode" originally determined by the second-order correction in the long-wave approximation of the transition $E\lambda$ operator in an electromagnetic field [10,32], and the other is the "vortical mode" in Ravenhall-Wambach's prescription [11]. Kvasil *et al.* described the general treatment of the toroidal, compressive, and vortical modes and their relation to each other [15]. They showed that the toroidal mode is a good probe for LE-ISD excitations rather than the vortical mode, though both the TD and the vortical dipole (VD) operators can measure the vorticity. In this paper, we mainly discuss the TD and CD transitions. We also show the VD transitions just for comparison.

We use the TD, CD, and VD operators defined in Ref. [15] as

$$M_{\mathrm{TD}}(\mu)=\frac{-i}{2\sqrt{3}c}\int d\boldsymbol{r}\,\boldsymbol{j}(\boldsymbol{r})\left[\frac{\sqrt{2}}{5}r^2\boldsymbol{Y}_{12\mu}(\hat{\boldsymbol{r}})+r^2\boldsymbol{Y}_{10\mu}(\hat{\boldsymbol{r}})\right], \tag{11}$$

$$M_{\mathrm{CD}}(\mu)=\frac{-i}{2\sqrt{3}c}\int d\boldsymbol{r}\,\boldsymbol{j}(\boldsymbol{r})\left[\frac{2\sqrt{2}}{5}r^2\boldsymbol{Y}_{12\mu}(\hat{\boldsymbol{r}})-r^2\boldsymbol{Y}_{10\mu}(\hat{\boldsymbol{r}})\right], \tag{12}$$

$$M_{\mathrm{VD}}(\mu)=\frac{-i}{2\sqrt{3}c}\int d\boldsymbol{r}\,\boldsymbol{j}(\boldsymbol{r})\left[\frac{3\sqrt{2}}{5}r^2\boldsymbol{Y}_{12\mu}(\hat{\boldsymbol{r}})\right], \tag{13}$$

where $\boldsymbol{j}(\boldsymbol{r})$ is the current density operator and $\boldsymbol{Y}_{\lambda L\mu}$ is the vector spherical harmonics. Using the dipole operators we analyze the toroidal nature of the dipole excitations in the same matter as done in Ref. [33], which discusses dipole excitations of ^{10}Be. The detailed definition of $\boldsymbol{j}(\boldsymbol{r})$ as well as that of the density operator $\rho(\boldsymbol{r})$ is explained in the Appendix in Ref. [33]. For the current density, we take into account only the convection part of the nuclear current but omit its magnetization (spin) part. The matrix elements for the dipole transitions, $|0_1^+\rangle\to|1_k^-\rangle$, are given with the transition current density $\delta\boldsymbol{j}(\boldsymbol{r})\equiv\langle 1_k^-|\boldsymbol{j}(\boldsymbol{r})|0_1^+\rangle$ as

$$\langle 1_k^-|M_{\mathrm{TD}}(\mu)|0_1^+\rangle=\frac{-i}{2\sqrt{3}c}\int d\boldsymbol{r}\,\delta\boldsymbol{j}(\boldsymbol{r})\times\left[\frac{\sqrt{2}}{5}r^2\boldsymbol{Y}_{12\mu}(\hat{\boldsymbol{r}})+r^2\boldsymbol{Y}_{10\mu}(\hat{\boldsymbol{r}})\right], \tag{14}$$

$$\langle 1_k^-|M_{\mathrm{CD}}(\mu)|0_1^+\rangle=\frac{-i}{2\sqrt{3}c}\int d\boldsymbol{r}\,\delta\boldsymbol{j}(\boldsymbol{r})\times\left[\frac{2\sqrt{2}}{5}r^2\boldsymbol{Y}_{12\mu}(\hat{\boldsymbol{r}})-r^2\boldsymbol{Y}_{10\mu}(\hat{\boldsymbol{r}})\right], \tag{15}$$

$$\langle 1_k^-|M_{\mathrm{VD}}(\mu)|0_1^+\rangle=\frac{-i}{2\sqrt{3}c}\int d\boldsymbol{r}\,\delta\boldsymbol{j}(\boldsymbol{r})\left[\frac{3\sqrt{2}}{5}r^2\boldsymbol{Y}_{12\mu}(\hat{\boldsymbol{r}})\right]. \tag{16}$$

Note that the CD matrix element can be transformed to an ordinary ISD matrix element (labeled IS1) by using the continuity equation $\nabla\cdot\boldsymbol{j}=-\frac{i}{\hbar}[H,\rho]$ as

$$\langle 1_k^-|M_{\mathrm{CD}}(\mu)|0_1^+\rangle=-\frac{E}{10\hbar c}\langle 1_k^-|M_{\mathrm{IS1}}(\mu)|0_1^+\rangle, \tag{17}$$

$$M_{\mathrm{IS1}}(\mu)\equiv\int d\boldsymbol{r}\,\rho(\boldsymbol{r})r^3Y_{1\mu}(\hat{\boldsymbol{r}}), \tag{18}$$

where E is the excitation energy of the 1_k^- state.

For the 0_1^+ and 1_k^- wave functions obtained by the sAMD + GCM, we calculate the transition strengths of the dipole operators,

$$\tilde{B}(\mathrm{TD,CD,VD};0_1^+\to1_k^-)\equiv\left(\frac{10\hbar c}{E}\right)^2|\langle 1_k^-||M_{\mathrm{TD,CD,VD}}||0_1^+\rangle|^2. \tag{19}$$

Here we define the transition strengths scaled with the factor $(\frac{10\hbar c}{E})^2$ so that $\tilde{B}(\mathrm{CD})$ corresponds to the IS1 strength $B(\mathrm{IS1})=|\langle 1_k^-||M_{\mathrm{IS1}}||0_1^+\rangle|^2$.

IV. RESULTS

A. Effective interactions

The adopted effective interactions are the same as those used in the previous work [29]. The central force is the MV1 force [34], consisting of two-range Gaussian two-body terms and a zero-range three-body term. As for the parametrization of the MV1 force, case 1 with the Bartlett, Heisenberg, and Majorana parameters, $b=h=0$ and $m=0.62$, is used. In addition to the central force, the two-range Gaussian spin-orbit term of the G3RS force [35,36] with strengths $u_I=-u_{II}=3000$ MeV is supplemented. This set of interaction parameters describes well the properties of the ground and excited states of ^{10}Be and ^{12}C in the AMD + VAP calculations [37–39]. For matter properties, the MV1 force with the present parameters gives the saturation density $\rho_s=0.192$ fm^{-3}, saturation energy $E_s=-17.9$ MeV, and incompressibility $K=245$ MeV.

V. ISD EXCITATIONS OF ^{12}C OBTAINED WITH THE sAMD + GCM

We calculate the TD, CD, and VD transitions from the ground to the 1^- states obtained with the sAMD + GCM. The calculated transition strengths are shown in Fig. 2(a). Remarkable TD and VD strengths are obtained for LED states in the $E=10$-15 MeV region, whereas the CD operator strengths are mainly distributed in the high-energy part corresponding to the ISGDR. The LE strengths are concentrated in two dipole states; one is the 1_1^- state at 12.6 MeV, which we assign to the experimental 1^-(10.844-MeV) state, and the other is the 1_2^- state at 14.8 MeV. The 1_2^- state has a significant 1p-1h component and is approximately described within the sAMD model space. On the other hand, the 1_1^- state has a spatially

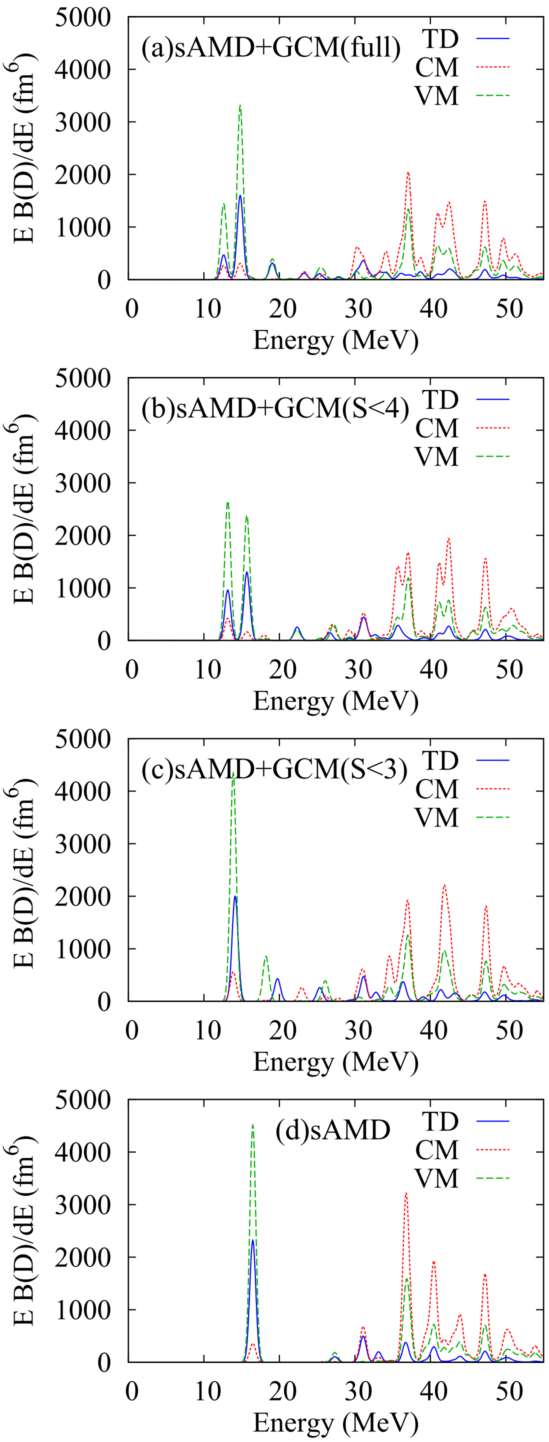

FIG. 2. Strength functions of the TD, CD, and VD transitions calculated with (a) the full sAMD + GCM, (b) the sAMD with $|\boldsymbol{S}_k| \leqslant 4$ fm 3α configurations, (c) the sAMD with $|\boldsymbol{S}_k| \leqslant 3$ fm 3α configurations, and (d) the sAMD without 3α configurations. The strengths of discrete states are smeared by a Gaussian with the range $\gamma = 1/\sqrt{\pi}$ MeV.

developed 3α-cluster structure, which is a high-amplitude cluster mode beyond the sAMD model space. This means that, in the 1^- spectra of ^{12}C, the high-amplitude cluster mode exists at an energy lower than the 1p-1h-dominant dipole excitation.

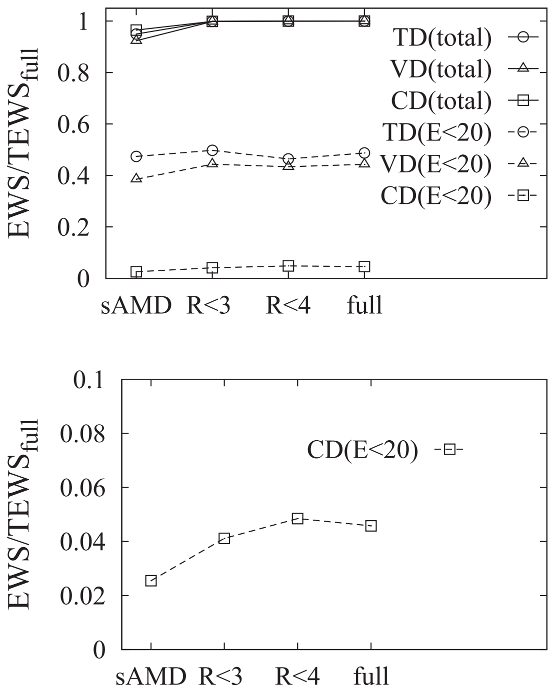

FIG. 3. Energy-weighted TD, VD, and CD strengths summed up to $E = 20$ MeV obtained with the sAMD, sAMD + GCM ($|\boldsymbol{R}_k| \leqslant 3$ fm), sAMD + GCM ($|\boldsymbol{R}_k| \leqslant 4$ fm), and full sAMD + GCM calculations. The ratio to the total energy weighted sum value of the full sAMD + GCM (TEWS$_{\text{full}}$) is shown. The TEWS value of each calculation relative to the TEWS$_{\text{full}}$ is also shown.

The 3α-cluster structure of the 1_1^- state is consistent with the 3α-GCM calculation in Refs. [21] and [22].

In order to see the significance of the high-amplitude cluster motion in the LE-ISD excitations, we perform calculations within truncated model spaces by reducing 3α configurations. Figures 2(b), 2(c) and 2(d) show the ISD strengths obtained with the truncated calculations using the sAMD with $|\boldsymbol{S}_k| \leqslant 4$ fm 3α configurations, the sAMD with $|\boldsymbol{S}_k| \leqslant 3$ fm, and the sAMD without 3α configurations, respectively. Note that $|\boldsymbol{S}_k|$ is the distance of the α_k-cluster center from the origin. In the calculations, the initial state is fixed to be the 0_1^+ state obtained by the full sAMD + GCM. As shown in Fig. 2(d), the sAMD without 3α configurations shows only one 1^- state in $E < 20$ MeV. The 1^- state has a dominant 1p-1h component with a remarkable TD strength and approximately corresponds to the 1_2^- state of the full sAMD + GCM. In the sAMD result, there is no low-lying 3α-cluster state corresponding to the 1_1^- state of the full sAMD + GCM. As 3α-cluster configurations are added to the sAMD model space, the 3α-cluster state appears around 20 MeV in the sAMD + GCM ($|\boldsymbol{S}_k| \leqslant 3$ fm) [Fig. 2(c)], comes down to 15 MeV in the sAMD + GCM ($|\boldsymbol{S}_k| \leqslant 4$ fm) [Fig. 2(b)], and, finally, becomes lower than the 1p-1h-dominant 1_2^- state in the full sAMD + GCM. In other words, as the high-amplitude intercluster motion develops, the cluster mode comes down to the lowest 1^- state crossing the 1p-1h state.

Figure 3 shows the EWS of the TD, VD, and CD strengths up to $E = 20$ MeV obtained in the truncated and full calculations.

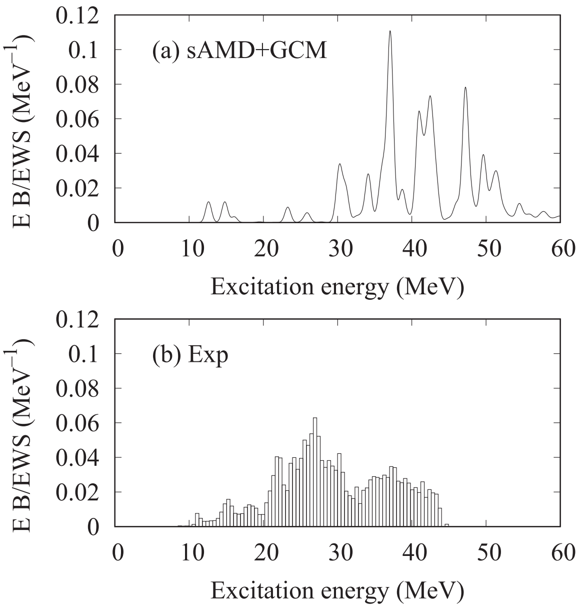

FIG. 4. EWSR ratio of the energy-weighted IS1 strengths. (a) Calculated strengths smeared by a Gaussian of width $\gamma = 1/\sqrt{\pi}$ MeV. (b) Experimental data measured by α inelastic scattering from Ref. [18]. Figures are from Ref. [29].

The ratio to the total energy-weighted sum of the full sAMD + GCM ($\mathrm{TEWS_{full}}$) is shown. The EWS value of the LE TD (VD) strengths is as much as 40%–50% of the TEWS almost independently of the truncation of the 3α configurations. This means that the sum of the LE TD strengths is approximately described by the 1p-1h configurations within the sAMD model space. As shown in Figs. 2(a) and 2(d), the strength of the LE TD transition is originally concentrated at the single peak in the sAMD, and it is split into two LED states in the full sAMD + GCM as a result of coupling with the high-amplitude 3α-cluster mode. By contrast, the LE CD transition strengths have only tiny percentages of the TEWS. The ratio is 2.5% in the sAMD, and it is raised to 4%–5% by 3α configurations. This means that about a half of the LE CD strengths is contributed by 1p-1h configurations and the other half comes from 3α configurations.

Figure 4 shows a comparison of the calculated IS1 strengths with the experimental data measured by α inelastic scattering. The calculated LE IS1 strengths are comparable to the experimental data. We assign the lowest peak for the calculated 1^-_1 state to the experimental IS1 strength for the 1^-_1 state (10.84 MeV). The bump structure around $E = 15$ MeV in the experimental strength function is a candidate for the calculated 1^-_2 state. In the present calculation, high-energy strengths for the ISGDR are distributed in the $E = 30$-50 MeV region. The calculated ISGDR energy seems more or less higher than the experimental ISGDR energy, though the strengths in the $E > 45$ MeV region have not been measured. A reason for the overestimation of the observed ISGDR energy might be that the present effective interactions give a larger value ($K = 245$ MeV) of the nuclear matter incompressibility than the standard value expected from the ISM energies in heavy nuclei. Another possible reason is the restriction of radial behavior of the present model wave function, in which only configurations up to $3\hbar\omega$ excited harmonic oscillator bases are taken into account because the sAMD wave function is expressed by shifted Gaussians with a fixed width.

VI. CLUSTER AND TOROIDAL NATURES OF LOW-ENERGY DIPOLE EXCITATIONS

In the present calculation, two LED modes are obtained at $E = 10$-15 MeV. One is the high-amplitude 3α-cluster mode, and the other is the 1p-1h-dominant dipole excitation. We here discuss the cluster and toroidal natures of the LED states.

A. Occupation probabilities in the shell-model expansion

Figure 5 shows the occupation probability of harmonic oscillator quanta N in the shell-model-basis expansion with size parameter $b = 1/\sqrt{2\nu}$. The dominant component of the 0^+_1 state is the $0\hbar\omega$ configuration, with 20% mixing of higher shell configurations. By contrast, the occupation probability of the 0^+_2 state is distributed broadly in the high shell region because of the spatially developed 3α-cluster structure. Similarly to the 0^+_2 state, the 1^-_1 state shows a very broad distribution of the occupation probability due to the developed cluster structure. The 1^-_2 state contains 40% $1\hbar\omega$ component, indicating dominant 1p-1h excitations with significant higher shell mixing.

B. Intrinsic structures

In the sAMD + GCM calculation, each state is expressed by superposition of many different configurations of the shifted AMD and 3α wave functions. For an intuitive understanding of the LED excitations, it is useful to consider a single Slater determinant which approximately describes the state

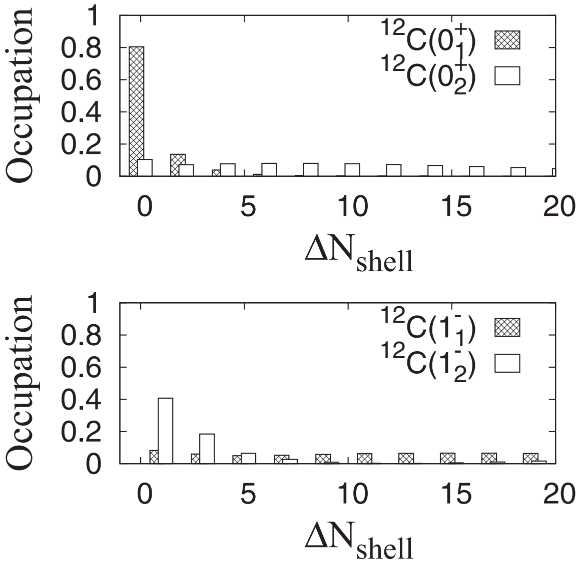

FIG. 5. Occupation probability of harmonic oscillator quanta N in the shell-model basis expansion of the $0^+_{1,2}$ and $1^-_{1,2}$ states obtained with the sAMD + GCM calculation. The horizontal axis indicates the difference ΔN from the minimum quanta $N_{\min} = 8$.

of interest. We here perform a simple model analysis by introducing model wave functions that have large overlap with the obtained 0_1^+, 1_1^-, and 1_2^- states in order to discuss the cluster and toroidal natures of the LED modes in the intrinsic frame.

As for the model wave functions in the present analysis, we adopt an extended 3α (E-3α) model based on the quasi-α-cluster model proposed by Itagaki *et al.* [40], in which the α-breaking is taken into account by the cluster-breaking parameter Λ. We start from the Brink-Bloch 3α-cluster wave functions and incorporate the breaking of the two α clusters, α_1 and α_2.

Let us first consider the $\theta = \pi/2$ case for an isosceles triangle 3α configuration. An E-3α wave function can be expressed by the AMD wave function with parameters

$$\boldsymbol{X}_i = \boldsymbol{S}_1 + i\boldsymbol{W}_i \quad (i = 1,\ldots,4), \tag{20}$$

$$\boldsymbol{X}_i = \boldsymbol{S}_2 + i\boldsymbol{W}_i \quad (i = 5,\ldots,8), \tag{21}$$

$$\boldsymbol{X}_i = \boldsymbol{S}_3 \quad (i = 9,\ldots,12), \tag{22}$$

$$\boldsymbol{W}_i = \Lambda\left(\boldsymbol{e}_{\sigma i} \times \frac{\boldsymbol{r}}{2}\right) \quad (i = 1,\ldots,4), \tag{23}$$

$$\boldsymbol{W}_i = \Lambda\left(\boldsymbol{e}_{\sigma i} \times \left(-\frac{\boldsymbol{r}}{2}\right)\right) \quad (i = 5,\ldots,8). \tag{24}$$

The spin and isospin functions are fixed to be $\tau_i\chi_i = p\uparrow$, $p\downarrow$, $n\uparrow$, and $n\downarrow$ for $i = \{1,5,9\}$, $i = \{2,6,10\}$, $i = \{3,7,11\}$, and $i = \{4,8,12\}$, respectively, and $\boldsymbol{e}_{\sigma i}$ indicates the unit vector for the spin orientation. Λ describes the α-breaking because of the spin-orbit interaction through the imaginary part $\boldsymbol{W}_i$ of the Gaussian centroid $\boldsymbol{X}_i$, which depends on the intrinsic spin orientation. In the $\Lambda > 0$ case, $\boldsymbol{W}_i$ indicates finite momenta of nucleons boosted by the spin-orbit potential. Next, a nonisosceles triangle 3α configuration is constructed by rotating the α_1 and α_2 clusters with angle $\pi/2 - \theta$ around $-\boldsymbol{D}/3$. Consequently, the E-3α wave function used here is specified by the parameters r, D, θ, and Λ. We denote the E-3α wave function $\Phi_{\text{E-}3\alpha}(r,D,\theta,\Lambda)$, which is expressed by a single Slater determinant. In the $\Lambda = 0$ case, the E-3α wave function becomes equivalent to the ideal Brink-Bloch 3α-cluster wave function without the α-breaking. This means that the E-3α wave function adopted here contains the Brink-Bloch 3α-cluster wave function and also the $^8\text{Be}+\alpha$–cluster wave function with a distorted ^{8}Be cluster.

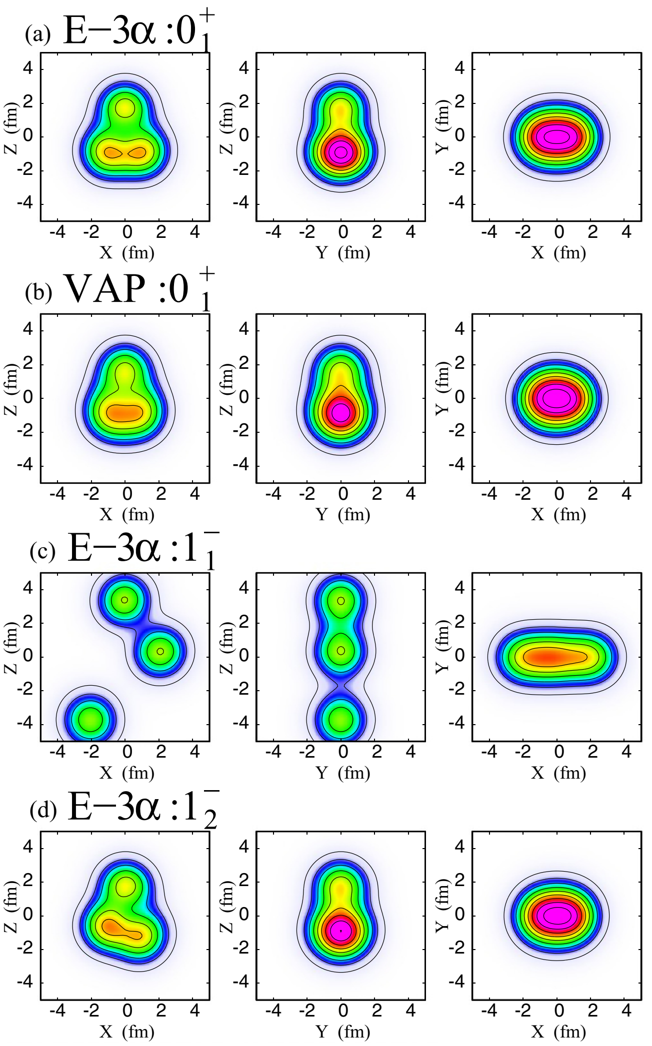

FIG. 6. Intrinsic density distributions of the dominant configurations written by the E-3α wave functions for the (a) 0_1^+, (c) 1_1^-, and (d) 1_2^- states. The intrinsic density of the AMD wave function $\Phi_{\text{AMD}}(\boldsymbol{Z}^0_{\text{VAP}})$ obtained with the VAP for the ground state is also shown. The density projected onto the X-Z, Z-Y, and X-Y planes by integrating along the axes perpendicular to the planes is shown. Contour lines are drawn with a 0.1-fm^{-2} interval.

We search for the E-3α wave functions that have a large overlap with the obtained 0_1^+, 1_1^-, and 1_2^- states and regard them as dominant configurations of the corresponding states. The intrinsic density distributions of the dominant configurations for the 0_1^+, 1_1^-, and 1_2^- states are shown in Fig. 6. The 0_1^+ state has 85% overlap with the 0^+-projected $\Phi_{\text{E-}3\alpha}$ with $r = 1$ fm, $D = 2$ fm, $\theta = \pi/2$, and $\Lambda = 0.5$, corresponding to a compact isosceles triangle structure with a significant α-breaking component. The E-3α wave function has almost the same structure as the AMD wave function obtained by the VAP for the 0_1^+ state. The 1_1^- state has 60% overlap with the $J^\pi K = 1^-1$–projected $\Phi_{\text{E-}3\alpha}$ with $r = 5.8$ fm, $D = 5$ fm, $\theta = \pi/4$, and $\Lambda = 0$ projected onto the $J^\pi K = 1^-1$ state, indicating the spatially developed 3α structure given by the Brink-Bloch 3α-cluster wave function. The 1_2^- state is the toroidal mode originally obtained as the 1_1^- state in the sAMD calculation. It has a large overlap with $\Phi_{\text{E-}3\alpha}$ with $r = 1$ fm, $D = 2$ fm, $\theta = 3\pi/8$, and $\Lambda = 0.5$ projected onto the $J^\pi K = 1^-1$ state and corresponds to a compact triangle configuration with cluster-breaking. It has 75% overlap with the 1p-1h-dominant TD mode of the sAMD. For the 1_2^- state in the sAMD + GCM, the overlap is reduced to 50% because of the coupling with the high-amplitude 3α-cluster mode. As shown in Fig. 6, the dominant configuration of the TD mode for the 1_2^- state shows an intrinsic structure similar to that of the 0_1^+ state except for the slight rotation (tilting) of the 2α part.

Figure 7 shows the transition current density for the transition between the dominant configurations of the 0_1^+ and 1_2^- states. The transition current density between the parity-

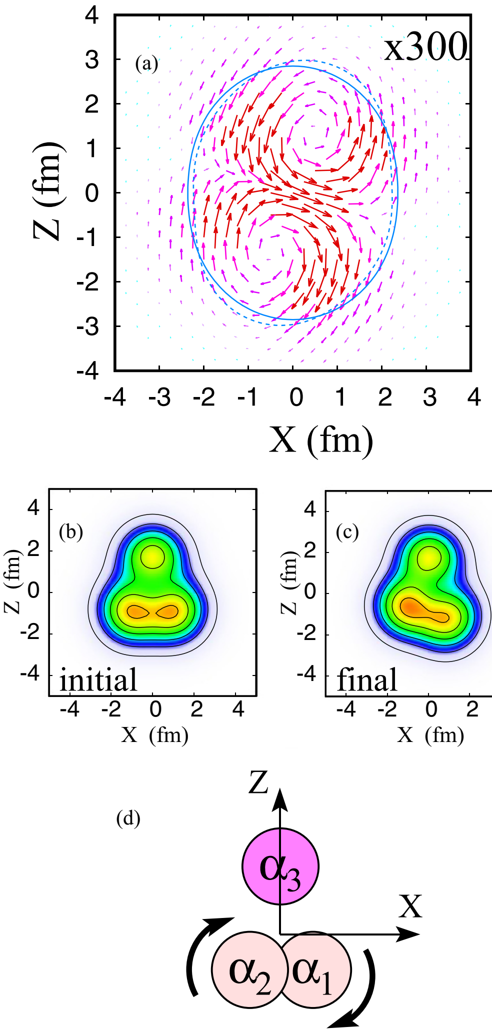

FIG. 7. (a) Transition current density for $0_1^+ \to 1_2^-$ in the intrinsic frame (at $Y = 0$ in the X-Z plane). The vector plot of the transition current density for the parity-projected states of the dominant E-3α configurations is shown. Solid red and dashed magenta lines indicate contours for the matter densities $\rho(X,0,Z) = 0.08\ \text{fm}^{-3}$ of the parity-projected initial and final states, respectively. (b) Intrinsic density distribution of the dominant configuration for the initial state (0_1^+) and (c) that for the final state (1_2^-). (d) Schematic of the $0_1^+ \to 1_2^-$ excitation in the cluster picture. α_1 and α_2 clusters contain cluster-breaking.

projected states of the dominant E-3α configurations,

$$\delta \boldsymbol{j}(\boldsymbol{r}) = \left\langle P^{\pi=-}\Phi_{\text{E-3}\alpha}\left(1_2^-\right) \left| \boldsymbol{j}(\boldsymbol{r}) \right| P^{\pi=+}\Phi_{\text{E-3}\alpha}\left(0_1^+\right)\right\rangle, \tag{25}$$

is shown in Fig. 7(a). Here, $\Phi_{\text{E-3}\alpha}(0_1^+)$ and $\Phi_{\text{E-3}\alpha}(1_2^-)$ are the dominant E-3α configurations of the 0_1^+ and 1_2^- states, respectively. The intrinsic densities without the parity projection of the initial and final configurations are shown again in Figs. 7(b) and 7(c). The transition current density clearly shows a toroidal nuclear current with the $K = 1$ feature in the prolately deformed intrinsic system and describes the remarkable TD strengths for the $0_1^+ \to 1_2^-$ transition. In a cluster picture, the toroidal current is understood by the rotation of the 2α subsystem as shown in the schematic in Fig. 7(d). This means that the 2α-cluster rotation induces TD-dominant dipole excitation. Note that the 2α subsystem in the initial and final states consists of not ideal α clusters but somewhat dissociated ones expressed by the α-breaking parameter $\Lambda = 0.5$ as mentioned previously.

A similar mechanism was found in ^{10}Be as discussed in Ref. [33]. In the case of ^{10}Be, the system can be approximately understood through the ^{6}He + α clustering, and the TD-dominant dipole excitation in the 1_1^- state is described by the rotation of the ^{6}He cluster. An interesting difference from ^{10}Be is that a high-amplitude cluster mode exists below the TD mode in the dipole excitations of ^{12}C.

C. TD mode in the shell-model limit

As discussed previously, the TD mode can be understood as the rotational excitation of the 2α subsystem. Instead of the cluster picture, it is worthwhile to discuss features of the TD mode in terms of 1p-1h excitations. Indeed, the 1_2^- state contains 40% $1\hbar\omega$ component as the dominant configuration, though it has significant mixing of higher shell components because of the coupling with the 3α-cluster state. We here consider the 1p-1h representation of the TD mode by taking a shell-model limit of the E-3α wave functions for the dominant configurations.

As explained previously, the ground state is approximately described by $\Phi_{\text{E-3}\alpha}$, with $r = 1$ fm, $D = 2$ fm, $\theta = \pi/2$, and $\Lambda = 0.5$ projected onto the $J^\pi = 0^+$ state, whereas the dominant component of the TD mode is described by $\Phi_{\text{E-3}\alpha}$, with $r = 1$ fm, $D = 2$ fm, $\theta = 3\pi/8$, and $\Lambda = 0.5$ projected onto the $J^\pi K = 1^-1$ state. By taking the limit of $\sqrt{\nu}r \ll 1$ and $\sqrt{\nu}D \ll 1$, we can map the dominant configurations to $0\hbar$ and $1\hbar\omega$ configurations in the shell-model limit for the ground state and the TD mode, respectively. For simplicity, we discuss the shell-model limit of the K^π-projected configuration in the intrinsic frame.

The shell-model limit of the E-3α wave function is represented by four-nucleon (4N: two protons and two neutrons) configurations around the SU(3)-limit 2α core with the $|000\rangle^4|001\rangle^4$ configuration. Here $|n_x n_y n_z\rangle$ means the single-particle state in the harmonic oscillator potential with the size parameter $b = 1/\sqrt{2\nu}$. For single-particle states around the $|000\rangle^4|001\rangle^4$ core, we use the following notation:

$$|p_{+\frac{3}{2}}\rangle = \frac{1}{\sqrt{2}}(|100\rangle + i|010\rangle)|\uparrow\rangle, \tag{26}$$

$$|p_{+\frac{1}{2}}\rangle = \frac{1}{\sqrt{2}}(|100\rangle + i|010\rangle)|\downarrow\rangle, \tag{27}$$

$$|p_{-\frac{1}{2}}\rangle = \frac{1}{\sqrt{2}}(|100\rangle - i|010\rangle)|\uparrow\rangle, \tag{28}$$

$$|p_{-\frac{3}{2}}\rangle = \frac{1}{\sqrt{2}}(|100\rangle - i|010\rangle)|\downarrow\rangle, \tag{29}$$

$$|sd_{+\frac{1}{2}}\rangle = |002\rangle|\uparrow\rangle, \tag{30}$$

$$|sd_{-\frac{1}{2}}\rangle = |002\rangle|\downarrow\rangle. \tag{31}$$

For the $K^\pi = 0^+$–and $K^\pi = 1^-$–projected states of the ground state (g.s.) and the TD mode, the 4N configurations in the shell-model limit are written as

$$\begin{aligned} P^+_{K=0}\Phi_{4N}(\text{g.s.}) = {}& \lambda_+^4 |p_{+\frac{3}{2}} p_{-\frac{3}{2}} p_{+\frac{3}{2}} p_{-\frac{3}{2}}\rangle |ppnn\rangle \\ &+ \lambda_+^2\lambda_-^2 |p_{+\frac{3}{2}} p_{-\frac{3}{2}} p_{+\frac{1}{2}} p_{-\frac{1}{2}}\rangle \\ &\times(|ppnn\rangle + |nnpp\rangle + |pnnp\rangle + |nppn\rangle) \\ &+ \lambda_-^4 |p_{+\frac{1}{2}} p_{-\frac{1}{2}} p_{+\frac{1}{2}} p_{-\frac{1}{2}}\rangle |ppnn\rangle, \end{aligned} \tag{32}$$

$$\begin{aligned} &P^-_{K=1}\Phi_{4N}(\text{TD}) \\ &= \lambda_+^4 (|p_{+\frac{3}{2}} sd_{-\frac{1}{2}} p_{+\frac{3}{2}} p_{-\frac{3}{2}}\rangle + |p_{+\frac{3}{2}} p_{-\frac{3}{2}} p_{+\frac{3}{2}} sd_{-\frac{1}{2}}\rangle)|ppnn\rangle \\ &\quad + \lambda_+^2\lambda_-^2 (|p_{+\frac{3}{2}} sd_{-\frac{1}{2}} p_{+\frac{1}{2}} p_{-\frac{1}{2}}\rangle + |p_{+\frac{3}{2}} p_{-\frac{3}{2}} p_{+\frac{1}{2}} sd_{+\frac{1}{2}}\rangle) \\ &\quad \times(|ppnn\rangle + |nnpp\rangle + |pnnp\rangle + |nppn\rangle) \\ &\quad + \lambda_-^4 (|p_{+\frac{1}{2}} sd_{+\frac{1}{2}} p_{+\frac{1}{2}} p_{-\frac{1}{2}}\rangle + |p_{+\frac{1}{2}} p_{-\frac{1}{2}} p_{+\frac{1}{2}} sd_{+\frac{1}{2}}\rangle)|ppnn\rangle, \end{aligned} \tag{33}$$

where $\lambda_+ : \lambda_- = (1+\Lambda) : (1-\Lambda)$. For simplicity, we here assume $r/\sqrt{\nu} \ll D/\sqrt{\nu} \ll 1$ and a θ value small enough to omit spin-flip excitations. It is shown that the shell-model limit for the ground state is not a simple paring state but a linear combination of correlating nn, pp, and np pairs in $p_{+3/2}p_{-3/2}$ and $p_{+1/2}p_{-1/2}$. Spin and isospin configurations are strongly correlated with each other because of the α-like correlation. The coefficients of the $p_{+3/2}p_{-3/2}p_{+3/2}p_{-3/2}$, $p_{+3/2}p_{-3/2}p_{+3/2}p_{-3/2}$, and $p_{+1/2}p_{-1/2}p_{+1/2}p_{-1/2}$ terms are determined by the α-breaking parameter Λ. The $\Lambda = 1$ case corresponds to the uncorrelated $4N$ state with the pure $p_{+3/2}p_{-3/2}p_{+3/2}p_{-3/2}$ configuration around the 2α core. The TD mode is expressed by 1p-1h excitations of $p^{-1}_{-3/2}sd_{-1/2}$ and $p^{-1}_{-1/2}sd_{+1/2}$ on top of the ground-state configuration. They are coherent 1p-1h excitations, changing the oscillator quanta $n_\perp \equiv n_x + n_y$ and n_z as $\Delta n_\perp = -1$ and $\Delta n_z = +2$, and contribute to the remarkably strong TD transition.

VII. SUMMARY AND OUTLOOK

We have investigated the cluster and toroidal natures of the ISD excitations in ^{12}C based on the sAMD + GCM calculation. In the E = 10-15 MeV region, we have found two LED modes. One is the spatially developed 3α-cluster state and the other is the TD mode. The TD mode is dominantly described by coherent 1p-1h excitations in the ground state. The cluster state comes down to an energy lower than the TD mode because of the high-amplitude cluster motion.

For CD (ordinary ISD) excitations, the transition strengths are mainly distributed in the high-energy region for the ISGDR, whereas 5% of the TEWS exists at $E < 20$ MeV, consistent with the experimental data. In the experimental data on the CD strengths, the bump structure at $E \sim 15$ MeV is a candidate for the 1^-_2 state of the 1p-1h-dominant TD mode. The LED states are strongly excited by the TD operator. In the present calculation, two modes, the cluster and TD modes, are coupled to each other. As a result of the coupling, the TD strengths for the 1^-_1 and 1^-_2 states are the same order. Unfortunately, there is no established method to experimentally observe the TD strengths.

We have discussed the feature of the TD mode from the cluster picture based on the model analysis by analyzing dominant configurations in the single-Slater expression. In the analysis, the transition current density clearly shows the toroidal nature of the TD mode induced by the rotation of the 2α-like deformed subsystem. We have also discussed the connection of the rotational excitation of the cluster with 1p-1h excitations by taking the shell-model limit of the dominant configurations. The TD mode can be understood as the coherent 1p-1h excitations in the ground state, in which spin and isospin configurations are highly correlated because of the α-type four-body correlation.

ACKNOWLEDGMENTS

The computational calculations in this work were performed using the supercomputer at the Yukawa Institute for Theoretical Physics, Kyoto University. This work was supported by JSPS KAKENHI Grants No. 26400270 and No. 16J05659.

---

[1] T. Yamada, Y. Funaki, T. Myo, H. Horiuchi, K. Ikeda, G. Ropke, P. Schuck, and A. Tohsaki, Phys. Rev. C **85**, 034315 (2012).
[2] Y. Chiba, M. Kimura, and Y. Taniguchi, Phys. Rev. C **93**, 034319 (2016).
[3] N. Paar, D. Vretenar, E. Khan, and G. Colo, Rep. Prog. Phys. **70**, 691 (2007).
[4] T. Aumann and T. Nakamura, Phys. Scripta **T152**, 014012 (2013).
[5] D. Savran, T. Aumann, and A. Zilges, Prog. Part. Nucl. Phys. **70**, 210 (2013).
[6] A. Bracco, F. C. L. Crespi, and E. G. Lanza, Eur. Phys. J. A **51**, 99 (2015).
[7] M. N. Harakeh and A. E. L. Dieperink, Phys. Rev. C **23**, 2329 (1981).
[8] P. Decowski, H. P. Morsch, and W. Benenson, Phys. Lett. **101**, 147 (1981).
[9] T. D. Poelhekken, S. K. B. Hesmondhalgh, H. J. Hofmann, A. van der Woude, and M. N. Harakeh, Phys. Lett. B **278**, 423 (1992).
[10] S. F. Semenko, Sov. J. Nucl. Phys. **34**, 356 (1981).
[11] D. G. Ravenhall and J. Wambach, Nucl. Phys. A **475**, 468 (1987).
[12] D. Vretenar, N. Paar, P. Ring, and T. Nikšić, Phys. Rev. C **65**, 021301 (2002).
[13] N. Ryezayeva, T. Hartmann, Y. Kalmykov, H. Lenske, P. von Neumann-Cosel, V. Y. Ponomarev, A. Richter, A. Shevchenko, S. Volz, and J. Wambach, Phys. Rev. Lett. **89**, 272502 (2002).
[14] P. Papakonstantinou, V. Y. Ponomarev, R. Roth, and J. Wambach, Eur. Phys. J. A **47**, 14 (2011).
[15] J. Kvasil, V. O. Nesterenko, W. Kleinig, P.-G. Reinhard, and P. Vesely, Phys. Rev. C **84**, 034303 (2011).
[16] A. Repko, P.-G. Reinhard, V. O. Nesterenko, and J. Kvasil, Phys. Rev. C **87**, 024305 (2013).

[17] V. O. Nesterenko, J. Kvasil, A. Repko, W. Kleinig, and P.-G. Reinhard, Phys. Atom. Nucl. **79**, 842 (2017).
[18] B. John, Y. Tokimoto, Y.-W. Lui, H. L. Clark, X. Chen, and D. H. Youngblood, Phys. Rev. C **68**, 014305 (2003).
[19] Y. Fukushima and M. Kamimura, J. Phys. Soc. Jpn. **44**, 225 (1978).
[20] M. Kamimura, Nucl. Phys. A **351**, 456 (1981).
[21] E. Uegaki, S. Okabe, Y. Abe, and H. Tanaka, Prog. Theor. Phys. **57**, 1262 (1977).
[22] E. Uegaki, Y. Abe, S. Okabe, and H. Tanaka, Prog. Theor. Phys. **62**, 1621 (1979).
[23] Y. Kanada-En'yo, H. Horiuchi, and A. Ono, Phys. Rev. C **52**, 628 (1995).
[24] Y. Kanada-En'yo and H. Horiuchi, Phys. Rev. C **52**, 647 (1995).
[25] Y. Kanada-En'yo and H. Horiuchi, Prog. Theor. Phys. Suppl. **142**, 205 (2001).
[26] Y. Kanada-En'yo, M. Kimura, and A. Ono, Prog. Theor. Exp. Phys. **2012**, 01A202 (2012).
[27] Y. Kanada-En'yo, Phys. Rev. C **89**, 024302 (2014).
[28] Y. Kanada-En'yo, Phys. Rev. C **93**, 024322 (2016).
[29] Y. Kanada-En'yo, Phys. Rev. C **93**, 054307 (2016).
[30] M. Kimura, Phys. Rev. C **95**, 034331 (2017).
[31] D. M. Brink, in *Proceedings of the International School of Physics Enrico Fermi, Course 36, Varenna*, edited by C. Bloch (Academic Press, New York, 1966).
[32] V. M. Dubovik and A. A. Cheshkov, Sov. J. Part. Nucl. **5**, 318 (1975).
[33] Y. Kanada-En'yo and Y. Shikata, Phys. Rev. C **95**, 064319 (2017).
[34] T. Ando, K. Ikeda, and A. Tohsaki, Prog. Theor. Phys. **64**, 1608 (1980).
[35] R. Tamagaki, Prog. Theor. Phys. **39**, 91 (1968).
[36] N. Yamaguchi, T. Kasahara, S. Nagata, and Y. Akaishi, Prog. Theor. Phys. **62**, 1018 (1979).
[37] Y. Kanada-En'yo, Phys. Rev. Lett. **81**, 5291 (1998).
[38] Y. Kanada-En'yo, H. Horiuchi, and A. Dote, Phys. Rev. C **60**, 064304 (1999).
[39] Y. Kanada-En'yo, Prog. Theor. Phys. **117**, 655 (2007); **121**, 895 (2009).
[40] N. Itagaki, H. Masui, M. Ito, and S. Aoyama, Phys. Rev. C **71**, 064307 (2005).